Supplementary Information

Visualization of crystallographic orientation and twist angles in two-dimensional crystals with an optical microscopy

Xueping Cui[1,2,5], Lulu Sun[1], Yan Zeng[1], Yang Hao[1,2], Yanpeng Liu[3], Dong Wang[4], Yuanping Yi[1], Kian Ping Loh[3*], Jian Zheng[1,5*], Yunqi Liu[1]

The epitaxial growth of n-tritriacontane crystallites on 2D crystals

Monolayer 2D crystals, including graphene, MoS_2, WS_2, $MoSe_2$, WSe_2, were grown by chemical vapor deposition (CVD) using methods reported previously.[1,2] The epitaxy growth of tritriacontane on these 2D crystals was performed by thermal evaporation deposition of tritriacontane. The oriented epitaxy of tritriacontane on 2D crystals was found to be highly reproducible both in the thermal evaporation deposition of ultra-high and low vacuum.

Method 1

20 mg of n-tritriacontane powder (Sigma Aldrich) in a quartz crucible was evaporated onto the 2D crystals in an organic evaporation system (made by MBRAUN). During deposition, a rate of 0.03 ± 0.02 Å/s was used and the 2D crystals were kept at room temperature, with a vacuum degree of 4×10^{-6} mbar. The deposited thickness of n-tritriacontane was recorded by a Rate/Thickness Monitor (STM-2XM) and the final deposited thickness of tritriacontane was 6 nm.

Method 2

As shown in Figure S1, about 30 mg of n-tritriacontane powder was placed at the bottom of a quartz tube in which the monolayer 2D crystals was set in the upper part. The quartz tube loaded with n-tritriacontane powder and 2D crystals was evacuated by an ordinary mechanical or molecular pump. When the vacuum degree in the quartz tube reached to 2×10^{-1} Pa, the tritriacontane powder at the bottom of the tube began to be heated to 80 ^{o}C. Discontinuing heating after 30 minutes and the deposition of

tritriacontane on the 2D monolayers was finished.

After deposition of tritriacontane, the 2D crystals were directly observed using an optical microscope without additional treatment. Rod-shaped oriented tritriacontane crystallites were demonstrated on the monolayer 2D crystals.

Mechanically exfoliated MoS_2 were peeled off from the bulk by an adhesive Scotch tape. The cleaved crystals on Scotch tape were then brought into contact with a SiO_2/Si substrate and slightly rubbed with a plastic tweezer to further peel off them. After removing the Scotch tape, monolayer MoS_2 crystals were left on the substrate. Bulk 2D crystals, including black phosphorus (BP), hexagonal boron nitride, InSe, Bi_2SeTe_2, SnS_2, TiS_2, TaS_2, NbS_2, $SnSe_2$, $TiSe_2$, $TaSe_2$, $NbSe_2$, ZrS_2, $ZrSe_2$, HfS_2, VS_2, were purchased from “2D AGE”. These bulk 2D crystals were cleaved in air using a Scotch tape to obtain thin 2D counterparts with fresh surface. Then the tritriacontane crystallites were epitaxially grown on these cleaved 2D crystals by thermal evaporation deposition. The deposition recipes were same to that of tritriacontane epitaxially grown on CVD-grown 2D crystals. Regular patterns of highly-oriented rod-shaped crystallites were directly observed with an optical microscope after deposition.

Fabrication of twisted MoS_2 bilayers

Monolayer MoS_2 crystals were grown on SiO_2/Si substrate by a CVD method. Highly oriented rodlike tritriacontane crystallites were epitaxially grown on monolayer MoS_2 by thermal evaporation. A 120 mg/mL of poly(methyl methacrylate) (PMMA)

solution was prepared by dissolving PMMA powder (Mw 996 000, Sigma Aldrich) in n-butyl acetate. The PMMA solution was spin-coated on tritriacontane-deposited MoS_2 monolayers at 2000 rpm for 60 s and dried in air. Then the PMMA-coated MoS_2 crystals with mark of tritriacontane crystallites were immersed into a 1 M/L solution of potassium hydroxide to etching the SiO_2/Si substrate. Three hours later, a freestanding film of PMMA / tritriacontane / MoS_2 was peeled off the substrate and washed three times by deionized water.

Stacking the freestanding film of PMMA / tritriacontane / MoS_2 on a tritriacontane crystallites-deposited MoS_2 crystal on SiO_2/Si substrate, with tritriacontane crystallites in the freestanding film rotated a desired angle to the tritriacontane crystallites on MoS_2 crystal on SiO_2/Si substrate, was followed. Then the PMMA layer and tritriacontane were dissolved in acetone, and the substrate was cleaned by isopropyl alcohol. A twisted MoS_2 bilayer was finally constructed in which a MoS_2 crystal was stacked onto another MoS_2 crystal with a desired twist angle.

The marker of tritriacontane crystallites enable 2D crystals of arbitrary shape, not limited to defined shaped single crystals grown by CVD, to be applicable to construct 2D bilayers with easily identified lattice orientation.

Energy analysis of tritriacontane molecules alignment on 2D crystals

In order to ascertain the most favorable adsorption position of tritriacontane molecules on the surface of 2D crystals, we performed a rotation potential energy scan. During the scan, single tritriacontane molecule as a rigid body was adsorbed on

2D crystals with its carbon backbone parallel to the surface of 2D crystals. Rotation potential energy curve of single tritriacontane molecule adsorbed on graphene, monolayer MoS_2 and black phosphorus were obtained respectively, as shown in Figure S3. A lowest energy was demonstrated along zigzag direction of 2D crystals, suggesting the thermodynamically most stable alignment of tritriacontane on 2D crystals. This is in good agreement with experimental observations.

All the density function theory (DFT) calculations were carried out by using the Vienna ab initio simulation package (VASP, version 5.4.1) with Perdew Burke Emzerhof (PBE) pseudopotential. The cutoff energy for the plane-wave basis set was set to be 400 eV and the Monkhorst-Pack k-mesh of $1 \times 1 \times 1$ was used. The van der Waals interactions between tritriacontane and the surface of 2D crystals were performed with Grimme's dispersion correction (D3).

Supplementary Figures

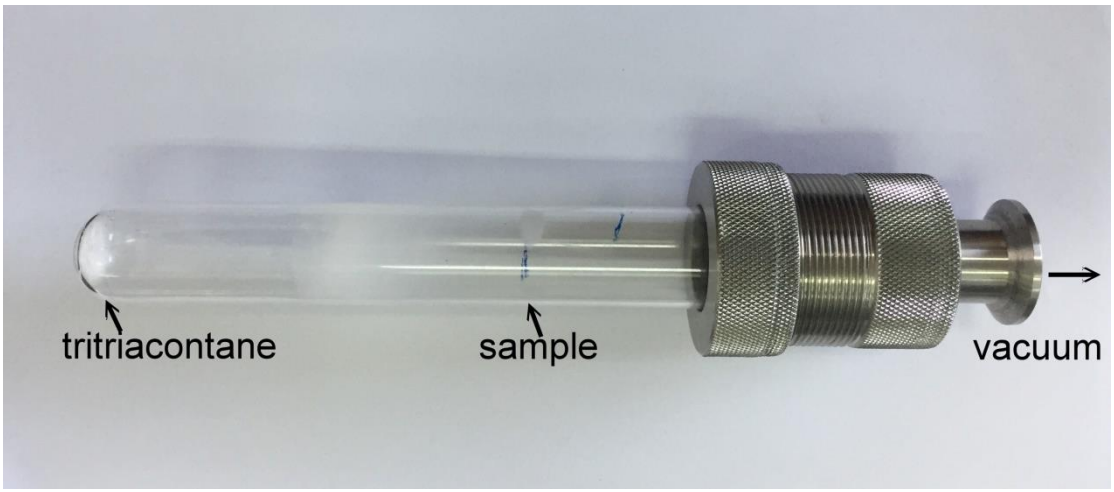

Figure S1. Photograph of the set-up for thermal evaporation of tritriacontane. Since it is not necessary for an ultra-high vacuum in the process of tritriacontane deposition, the system is evacuated by an ordinary mechanical or molecular pump.

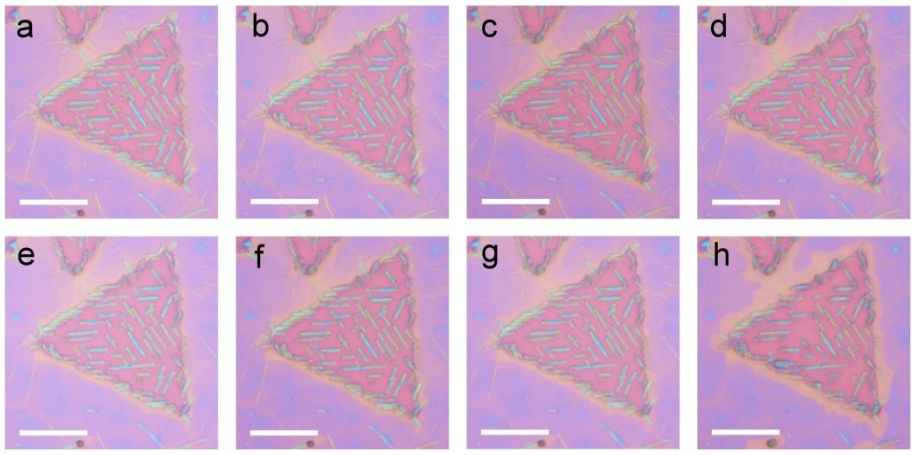

Figure S2. The evolution of tritriacontane crystallites on MoS_2 crystals in air. Optical images of MoS_2 crystals in air after the deposition of tritriacontane for 0 day (a), 1 day (b), 2 days (c), 3 days (d), 4 days (e), 5 days (f), 7 days (g) and one month (h). (Scale bars, 10 μm).

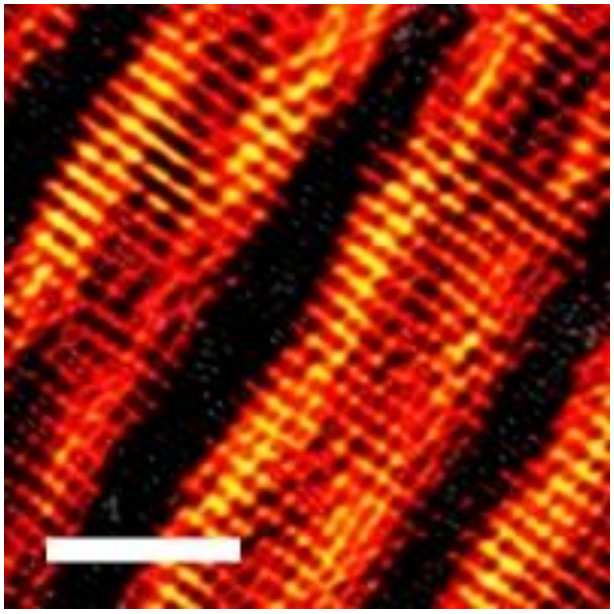

Figure S3. STM image of tritriacontane-deposited graphene. (V_{bias} = 700 mV; I_t = 500 pA; Scale bar, 3.7 nm)

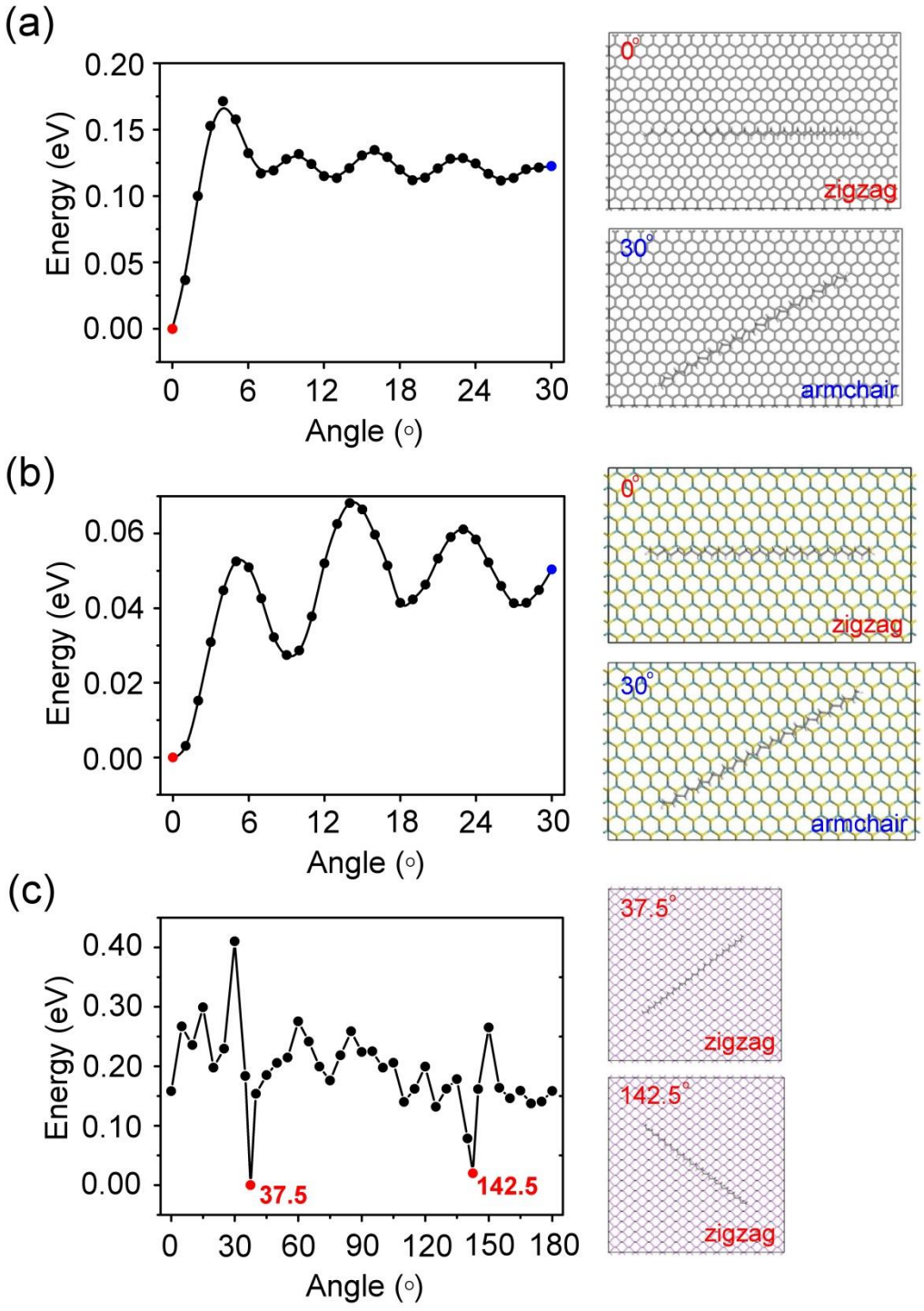

Figure S4. Rotation potential energy curve of single tritriacontane molecule adsorbed on graphene (a), MoS_2 (b) and black phosphorus (c).

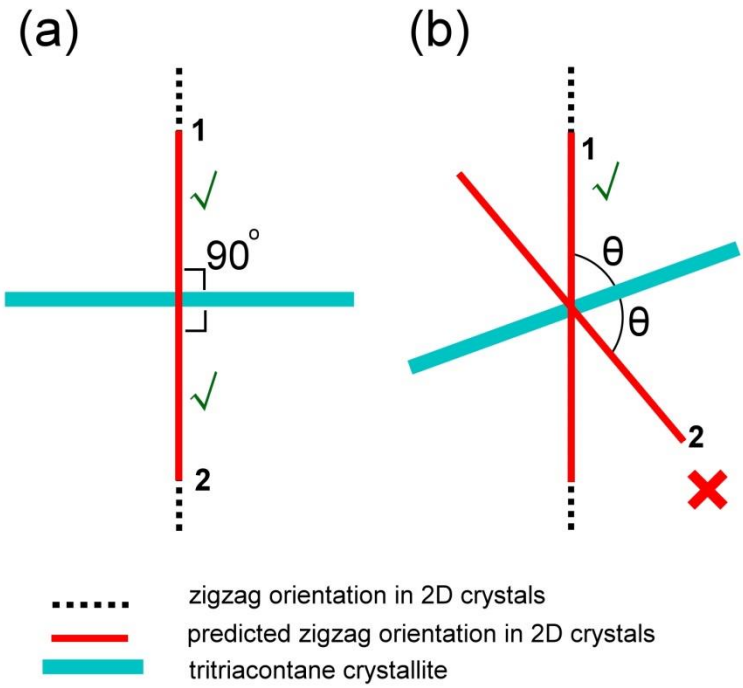

Figure S5. Schematics of indicating crystallographic orientation in 2D crystals by epitaxially grown orthonormal tritriacontane crystals (a) and other non-orthogonal crystals (b). When epitaxially grown on 2D crystals, tritriacontane molecule chain aligns along the zigzag direction of lattice structure of 2D crystals (black dotted line), thermodynamically most stable alignment as displayed in main text. For a rodlike tritriacontane crystallite of orthonormal polymorph, its molecule chain axis direction is perpendicular to the longitudinal direction of the crystal. Thus the zigzag direction of lattice structure of 2D crystals, that is molecule chain axis direction of tritriacontane, can be predicted by rotating the rod crystallite (green rod) 90 degrees from its longitudinal direction. Two rotating paths of the tritriacontane crystallite exist but the final predicted orientation of the 2D crystal is same and only, as shown in (a). While for a non-orthogonal crystal, zigzag direction of lattice structure of 2D crystals is obtained by rotating the rod crystallite (green rod) θ from its longitudinal direction. θ is the angle between the molecule chain axis and longitudinal direction of the crystal. Two different directions are predicted, bringing an uncertain determination of crystallographic orientation in 2D crystals, as shown in (b).

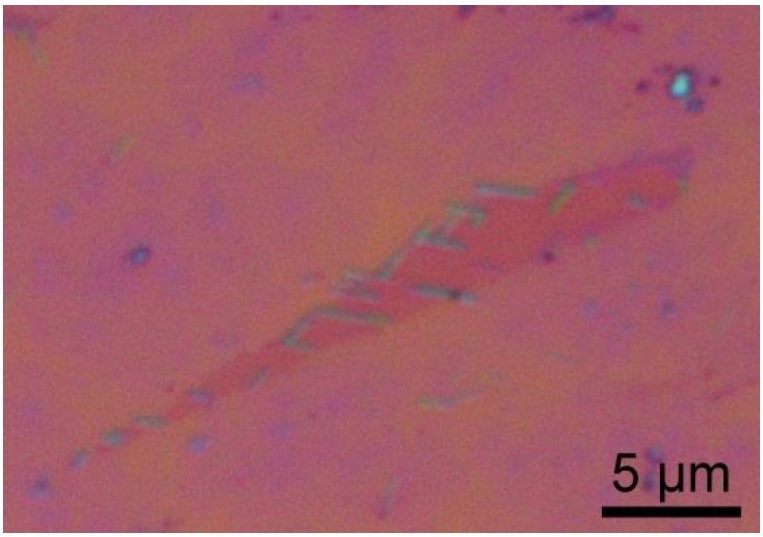

Figure S6. Optical image of a mechanically exfoliated monolayer MoS_2 flake with highly oriented tritriacontane crystallites.

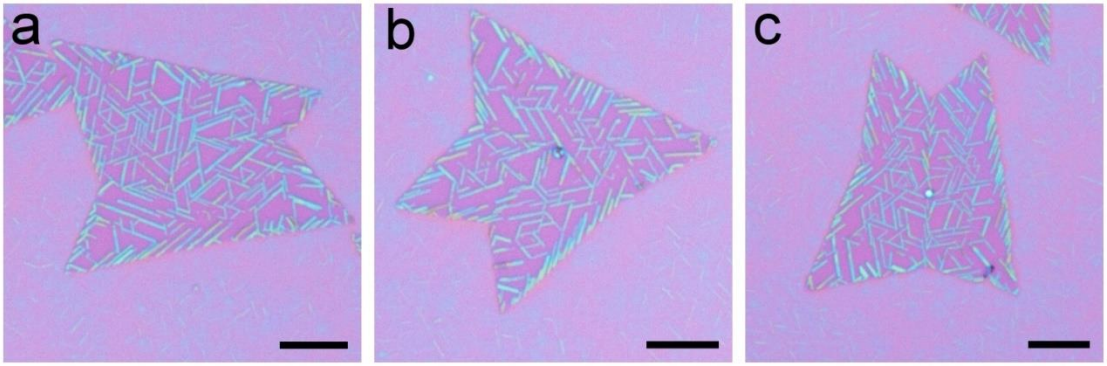

Figure S7. Identification of grain boundaries in CVD-grown MoS_2 crystals by tritriacontane epitaxy. Optical images of three different polycrystalline domains with epitaxially grown tritriacontane were shown in (a) to (c). The grain boundaries were clearly distinguishable due to a higher nucleation density of tritriacontane crystallites at the grain boundary. (Scale bars, 10 μm)

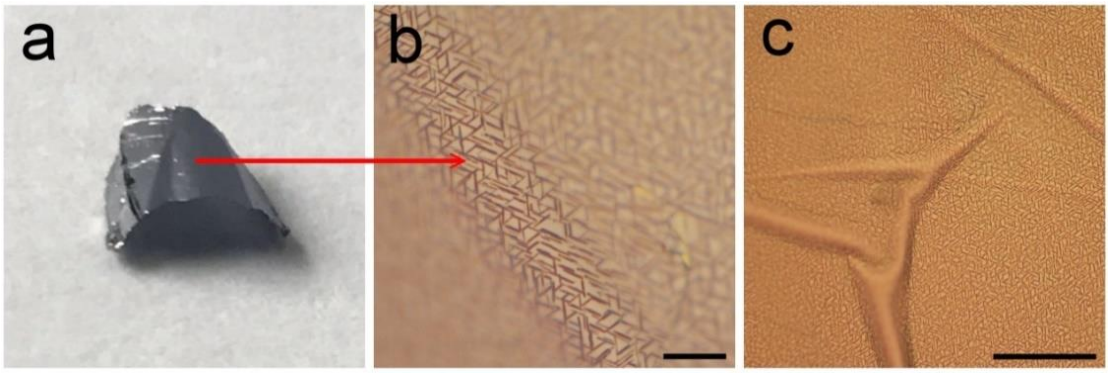

Figure S8. Oriented epitaxy growth of tritriacontane on MoS_2 crystals with wrinkled or curved surface. (a) Photograph of a curved MoS_2 crystals with epitaxially grown tritriacontane crystallites. (b) Optical image of the curved area in (a). (c) Optical image of a wrinkled MoS_2 crystal with epitaxially grown tritriacontane crystallites. (Scale bars, 10 μm in (b) and 50 μm in (c))

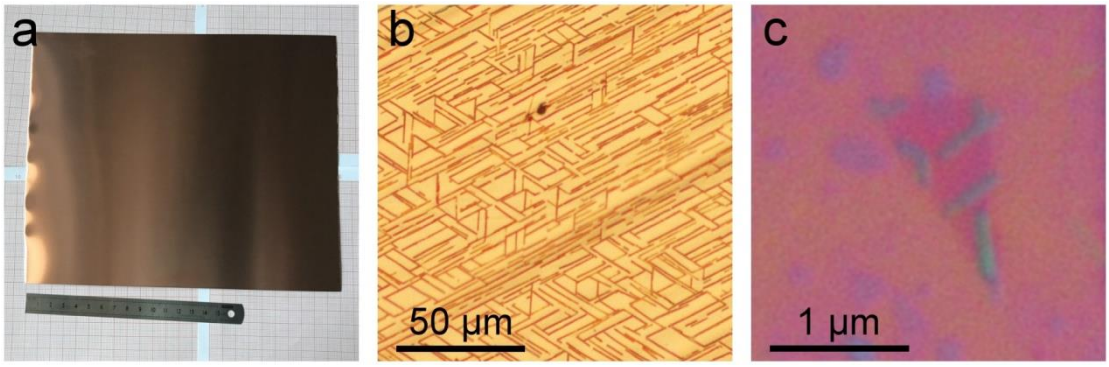

Figure S9. (a) Photograph of a large-area graphene on copper foil after epitaxial growth of tritriacontane. (b) Optical image of the red dot area in (a). The determination technique based on tritriacontane epitaxy allow a large-area and rapid determination of crystallographic orientation in 2D crystals by an ordinary optical microscope. (c) Optical image of a tritriacontane-oriented monolayer MoS_2 flake with a lateral dimension of about 1 μm.

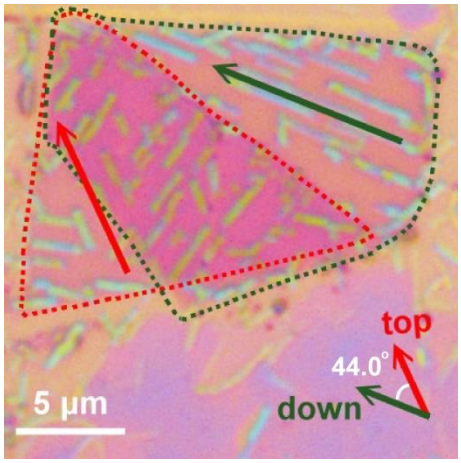

Figure S10. Observation of crystallographic orientations in an irregularly shaped MoS_2 bilayer with tritriacontane epitaxy. The two layers of MoS_2 in the bilayer were respectively indicated by red and green dashed lines and they were easily distinguished by tritriacontane crystallites of different oriented directions. The oriented direction of tritriacontane crystallites on each MoS_2 layer was indicated by red and green arrows respectively. The tritriacontane crystallites on the overlapped area of the bilayer share the same orientation with that on the left MoS_2 layer, indicating the top layer in the bilayer. It offers an easy identification of the stacking order in the bilayer under an optical microscope, as well as the crystallographic orientations. Based on the specific epitaxy relationship between tritriacontane and the 2D crystal, a twist angle of 44.0 degrees for the irregularly-shaped bilayer was obtained by measuring the angle between longitudinal directions of the tritriacontane crystallites respectively grown on each of the stack MoS_2 layer.

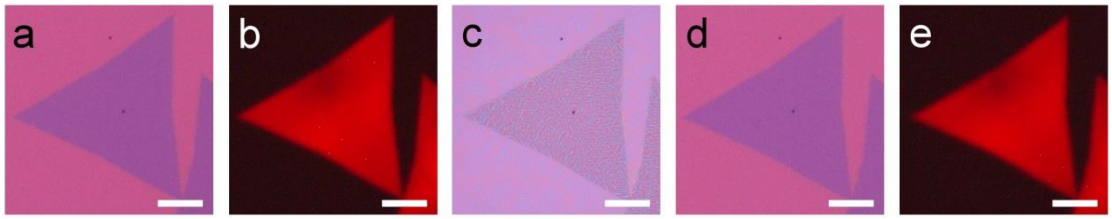

Figure S11. (a) Optical image of a original MoS_2 single crystal grown by chemical vapor deposition on a SiO_2/Si substrate. (b) Corresponding fluorescence image of the MoS_2 crystal in (a). (c) Optical image of MoS_2 single crystal in (a) with oriented epitaxy of tritriacontane. (d) Optical image of tritriacontane-deposited MoS_2 single crystal in (c) after heated at 80 ^{o}C in vacuum. (e) Corresponding fluorescence image of MoS_2 crystal in (d). The fluorescence images were obtained with an excitation wavelength of 510-560 nm. Scale bars, 20 μm in (a-e).

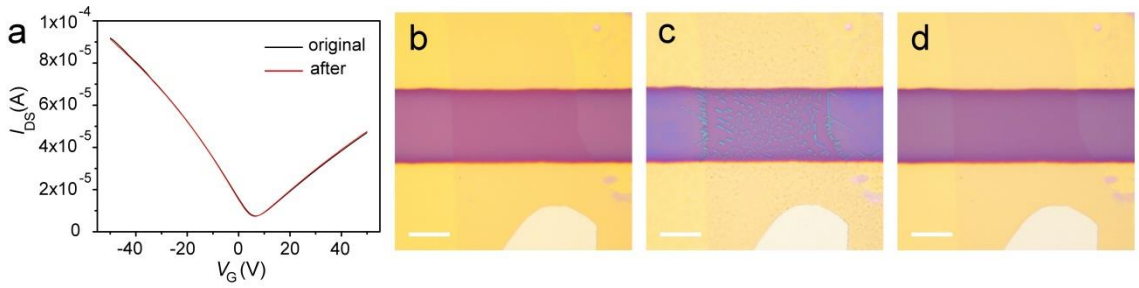

Figure S12. (a) Transfer characteristics of field effect transistor (FET) for original graphene (black line) and the same device after tritriacontane removal (red line). (b) Optical image of the graphene device before tritriacontane deposition. (c) Optical image of graphene device in (b) after tritriacontane deposition. (d) Optical image of graphene device in (c) after the tritriacontane removal. All the electrical characterization was conducted in N2. (Scale bars, 10 μm).

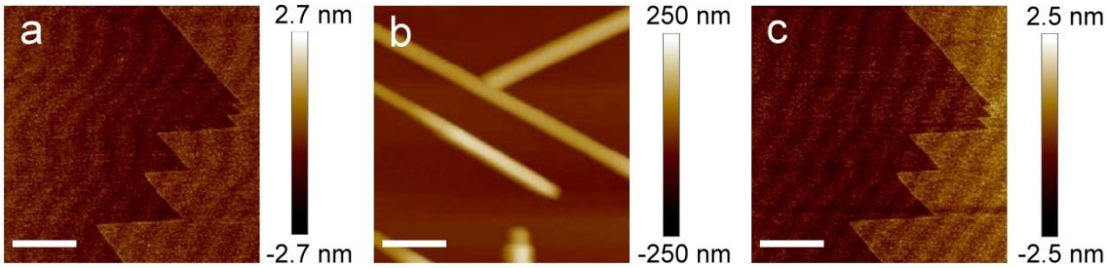

Figure S13. (a) AFM image of the surface of freshly exfoliated $TaSe_2$ flakes before the deposition of tritriacontane. (b) AFM image of the surface of $TaSe_2$ flakes in (a) after the deposition of tritriacontane. Rod-shaped tritriacontane crystallites were highly oriented on the surface of $TaSe_2$ flakes. Note that the tritriacontane crystallites had a height of around 100 nm, which were too high to the steps (less than 1 nm high) on the surface of original $TaSe_2$ flakes. Therefore, the steps on the original $TaSe_2$ flakes were covered after the deposition of tritriacontane. (c) AFM image of the surface of $TaSe_2$ flakes in (b) after the removal of tritriacontane. To minimize the effect of the air, the process of tritriacontane deposition and removal, and the AFM measurement were conducted in the glove box. (Scale bars, 1 μm).

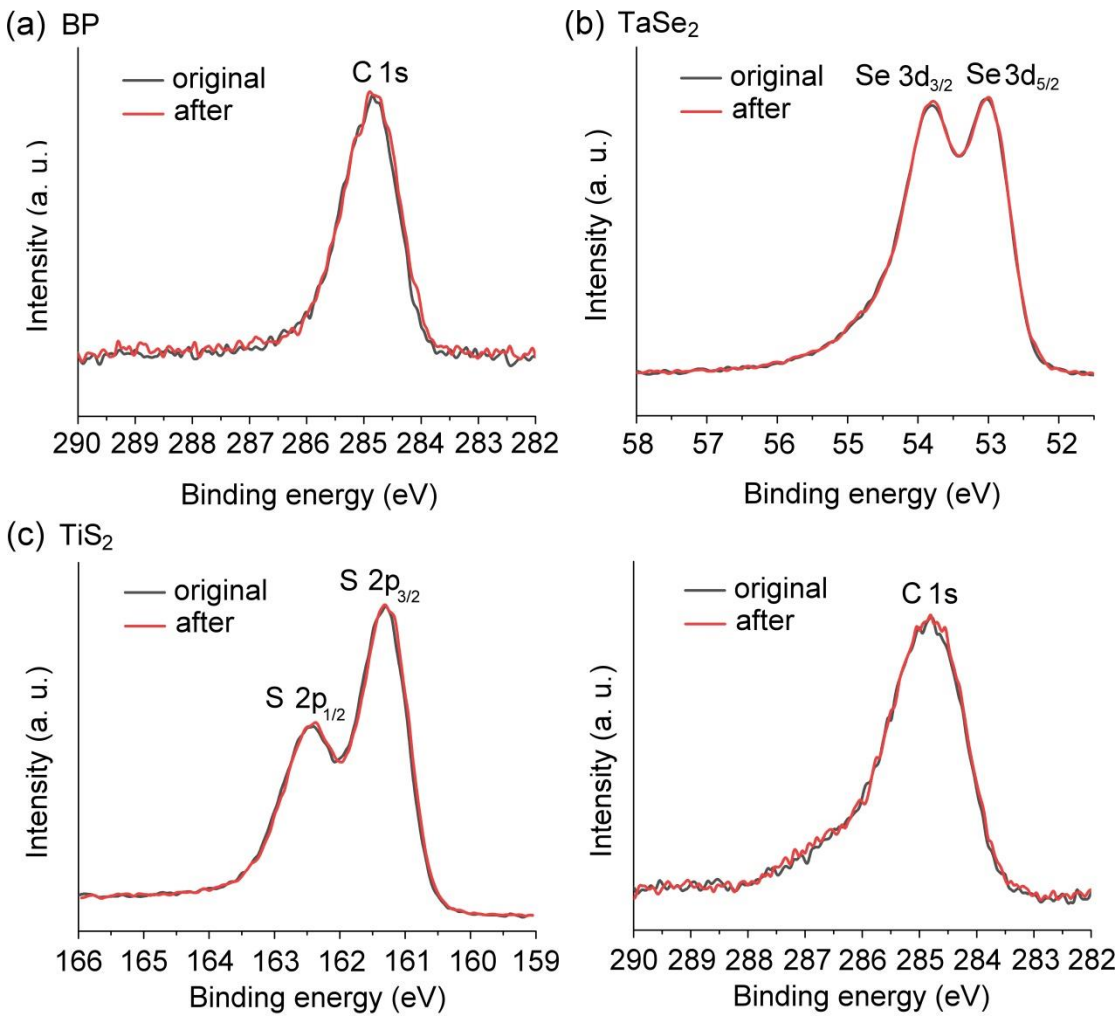

Figure S14. XPS spectra of BP (a), $TaSe_2$ (b) and TiS_2 (c) before tritriacontane deposition and after their removal.

The XPS was performed on the Thermo Scientific ESCALab 220i-XL using 200 W Al Kα or Mg Kα radiations. The 1 cm X-ray spot was used and the base pressure in the analysis chamber was about 5×10^{-9} mbar. The hydrocarbon C1s line at 284.8 eV from adventitious carbon was used for energy referencing.

To avoid air oxidation to 2D crystals, the process of 2D crystal exfoliation, tritriacontane deposition and removal were all performed in a glove box, with half-in situ XPS measurements. XPS spectra in Figure 5g showed the band associated with the P 2p at about 130 eV, which divided into P $2p_{1/2}$ (131eV) and P $2p_{3/2}$ (130.2 eV),

as a key feature of crystalline BP. The sub-band at about 136 eV related to the oxidized phosphorus (PO_x) was not detected after the removal of tritriacontane, indicating a well preservation of structural integrity of BP during the deposition and removal of the tritriacontane. The metallic $TaSe_2$ and TiS_2 displayed the similar behavior. As shown in the XPS spectra, no new band ascribed to the high oxidation state appeared after the removal of tritriacontane. The atomic ratio of Ta: Se in the $TaSe_2$ was measured to be 1:1.99 and 1:1.97 respectively before and after the tritriacontane epitaxy, both consistent with the stoichiometric ratio (1:2) of $TaSe_2$. In the TiS_2, the measured atomic ratio of Ti: S was 1:2.01 and 1:2.03 respectively before and after the tritriacontane epitaxy, corresponding to the stoichiometric ratio (1:2) of TiS_2. Similar C 1s peaks were demonstrated in the XPS of original BP and tritriacontane-removed BP (Figure S14a), with an almost unchanged carbon atomic ratio of 9.57 (original) and 9.74 (after). It suggested little absorption of tritriacontane on the surface of BP after the entire process. Little absorption of tritriacontane was also displayed in the TiS_2 (Figure S14c), where the carbon atomic ratios were 11.75 (original) and 11.77 (after). As for $TaSe_2$, due to the interference of Auger peaks of Se, it was hard to quantify the carbon in the $TaSe_2$ from the C 1s. But it can still figure out that the amount of carbon was little, leading to a weak C 1s signal overlapped with the Auger peak of Se.

References

1 L. Gao, G-X. Ni, Y. Liu, B. Liu, A. H. C. Neto, K. P. Loh. Face-to-face transfer of wafer-scale graphene films. *Nature* **2014**, 505, 190–194.

2 X. Cui, Z. Kong, E. Gao, D. Huang, Y. Hao, H. Shen, C-A. Di, Z. Xu, J. Zheng, D. Zhu. Rolling up transition metal dichalcogenide nanoscrolls via one drop of ethanol. *Nat. Commun.* **2018**, 9, 1301.